

# DFT Simulations of Titanium Oxide Films on Titanium Metal

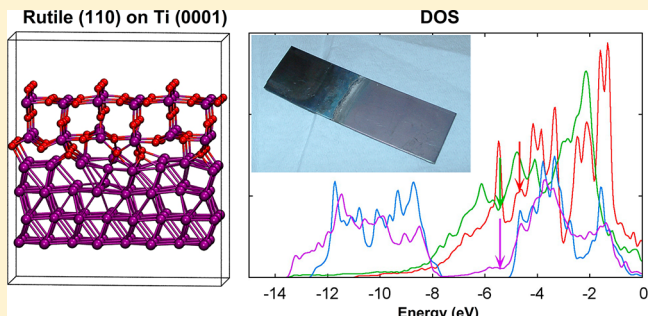
Bastian Ohler,<sup>†</sup> Stefano Prada,<sup>‡</sup> Gianfranco Pacchioni,<sup>‡</sup> and Walter Langel\*,<sup>†</sup>

<sup>†</sup>Institut für Biochemie, Universität Greifswald, Felix-Hausdorff-Strasse 4, 17487 Greifswald, Germany

<sup>‡</sup>Dipartimento di Scienza dei Materiali, Università degli Studi di Milano, Bicocca, Italy

## Supporting Information

**ABSTRACT:** Titanium surfaces in implants are covered by titanium oxide passivation layers of 1.5–25 nm thickness. At the surface  $\text{TiO}_2$  phases form with anatase and rutile structures. To improve the understanding of the initial phases of passivation, we investigated the interfaces between Ti and the most common oxide surfaces rutile (110) and (100) and anatase (101) and (001). Simulations based on a DFT+U approach revealed the presence of metal induced gap states (MIGS) caused by oxygen atoms that have moved toward the metal phase. We discuss the structural disorder around the interface and its effect on the oxide crystal structure. The computed work of separation is 3.4–4.3 J/m<sup>2</sup> which is much higher than the surface energies of Ti metal and  $\text{TiO}_2$  and results in a negative interface energy. Charge transfer takes place from the metal to the oxide and appears to be less dependent on the oxide phase than on the thickness of the slabs. We computed a charge transfer of 0.07 e per atom, most of which remains located in the first interface layers. The metal work function changes as a consequence of the formation of the passivation layer, but  $\Delta\Phi$  is positive for rutile and negative for anatase.



## 1. INTRODUCTION

When exposed to air titanium surfaces become covered by  $\text{TiO}_2$  passivation layers of 1.5–25 nm thickness.<sup>1–3</sup> During the passivation process stoichiometric phases like  $\text{TiO}$ ,  $\text{Ti}_2\text{O}_3$ , and other titanium oxides are formed only under high temperature and very low oxygen pressure.<sup>4</sup> Since typical experiments are performed at very low pressure (UHV), there are numerous reports of such phases.<sup>5–13</sup> After oxidation of bulk titanium at ambient temperatures  $\text{TiO}_2$  is the only detectable oxide.<sup>4,14,15</sup> When growing a titanium film on pure  $\text{TiO}_2$  crystals, amorphous interfaces of only a few monolayers thickness between the crystals have been detected via XPS.<sup>16</sup> The oxidation of initially pure titanium surfaces has been simulated by successively adding  $\text{O}_2$  molecules.<sup>17</sup> This approach produced amorphous  $\text{TiO}_x$  layers, but the formation of bulk crystalline  $\text{TiO}_2$  structures could not be reproduced within the time scale of atomistic simulations.

The dominant phases of  $\text{TiO}_2$  are rutile with its most stable surface orientations (110) or (100) and anatase with (101) or (001) surfaces, respectively. Experimentally, one finds the coexistence of both oxides.<sup>18–20</sup> The formation of each phase is dependent on annealing temperature,<sup>21–23</sup> particle size,<sup>24–26</sup> and shape.<sup>27</sup>

Bulk  $\text{TiO}_2$  is a semiconductor with a 3.1 eV band gap<sup>16</sup> averaging over rutile (3.0 eV) and anatase (3.2 eV),<sup>28</sup> but in most theoretical works, the observed band gaps are about 1 eV lower due to the well-known limitations of standard DFT approaches.<sup>29–31</sup> Experiments show that the introduction of oxygen vacancies creates defect states in the band gap about 0.8 eV below the bottom of the conduction band (CB).<sup>32,33</sup> The

defects are assigned to  $\text{Ti}^{3+}$  3d states by electron paramagnetic resonance (EPR) experiments.<sup>34–36</sup> In standard DFT calculations, however, the defect states of oxygen vacancy in  $\text{TiO}_2$  are located in the conduction band and the excess electrons are delocalized over several Ti ions.<sup>37,38</sup> This failure has recently been reviewed.<sup>39,40</sup> Practical ways to correct some of these deficiencies are based on hybrid functionals or the so-called DFT+U approach.<sup>29,41–44</sup> The latter avoids an additional Hartree–Fock calculation of the exchange energy but suffers from being dependent on the value of the U parameter.

Reference 29 reported different behavior of bulk rutile and anatase on the formation of an oxygen vacancy. Although in rutile only localized states in the middle of the band gap form, anatase has delocalized states at the bottom of the conduction band as well. Consequently the Fermi level of rutile ends up in the band gap and that of anatase in the conduction band. Different solutions, localized or delocalized, are often very close in energy.

The experimental and simulated work functions of Ti (0001) are in the range of 4.45–4.6 eV.<sup>45–47</sup> At higher oxygen exposure the work function increases by 0.8–1.0 eV, but some experimental and theoretical papers report an initial decrease in work function by up to 0.24 eV for small amounts of oxygen,<sup>46,48–51</sup> which has been reproduced theoretically.<sup>52</sup>

Experimental work function values for rutile range from 4.13<sup>53</sup> to 5.5 eV,<sup>54</sup> and ref 31 calculated a value of 6.83 eV.

**Received:** October 4, 2012

**Revised:** December 6, 2012

**Published:** December 10, 2012

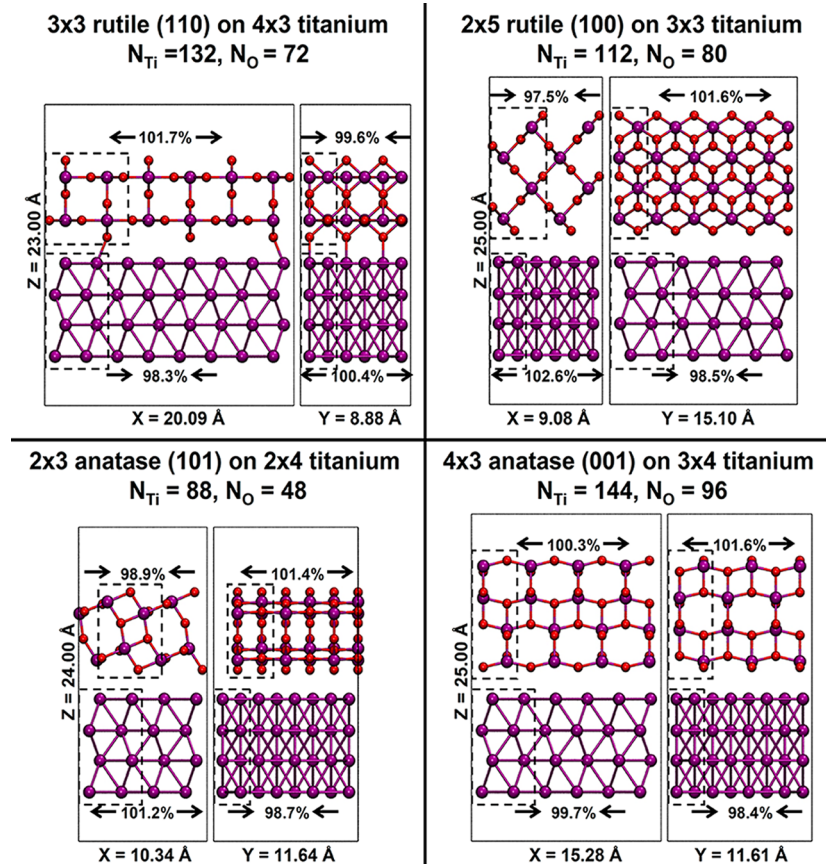


**Figure 1.** Starting structures of the interface models between the four  $\text{TiO}_2$  surfaces (magenta, Ti; red, O), titled according to the multiplicities of the smallest repetitive units in the  $x$  and  $y$  dimensions (dashed rectangles). The scaling factors for alignment of each phase are given as the number between arrows. The periodic boxes are indicated as full rectangles, and their sizes in all three dimensions are given. Each structure is displayed from two sides, looking along the  $y$  axis (left) and the  $x$  axis (right).

Anatase values range from  $4.77^{55}$  to  $5.4$  eV.<sup>56–58</sup> Values for different surface orientations thus overlap.

An important consequence of the deposition of a thin insulating film on a metal is the induced change in the metal work function, which can be reduced or increased depending on the nature of the interface.<sup>59</sup> When the metal wave function decays into the dielectric in the energy range where the metal conduction band overlaps with the band gap of the insulator,<sup>60</sup> metal induced gap states (MIGS)<sup>61–64</sup> appear. These may be caused by formation of true chemical bonds at the interface with donor- or acceptor-like character.<sup>64</sup> The presence of other states at the interface induces charge transfer across the interface leading to polarization. This increases the metal Fermi energy  $E_F$  if charge is transferred toward the metal, and reduces  $E_F$  in the reversed direction. Another effect that causes changes in the work function is the compression of metal electron density enforced by the oxide layer with subsequent change in surface dipole.<sup>59,65</sup> Work function changes are not just determined by the amount and the sign of the charge transferred but also by the details of charge distribution, leading in some cases to strong dependence of  $\Delta\Phi$  on the substrate orientation.<sup>66</sup>

During the initial phases of titanium surface oxidation, a thin  $\text{TiO}_2$  layer forms, influencing further oxygen diffusion into the metal. Analysis of the reactivity at the  $\text{Ti}/\text{TiO}_2$  interface is a complex task, and first-principles computations play an important role. The initial relaxation can be modeled in the time frame of ab initio simulations, providing detailed insights

into the atomic and electronic structure hardly accessible in the experiment.

In this work, we want to investigate how far metal and oxide properties are affected by the contact, regarding structural relaxation, atomic charges, and work function. This determines how far the influence of metal has to be considered in simulations of  $\text{TiO}_2$  passivation layers.<sup>67–72</sup> We earlier simulated the contact angle of water on oxides and reported a relationship to the surface charge.<sup>73</sup> This effect is obviously related to the photosensitivity of passivated titanium. In our force field simulations the nature of the electronic states involved could not be traced, however. We are also interested in the origin of the scatter of experimental values for the work function change  $\Delta\Phi$  induced by the oxide layer and to what extent this is related to structural disorder and polymorphy in the passivation layer.

## 2. METHODS

We used the Vienna ab initio simulation package (VASP),<sup>74,75</sup> which performs an iterative solution of the Kohn–Sham equations with a plane-wave basis set. The energy cutoff for plane waves was 300 eV.

The dynamic relaxation was carried out using ultra soft pseudopotentials with LDA (local-density approximation) and the Ceperly Alder functional parametrized by Perdew and Zunger<sup>76</sup> as implemented in VASP. Ten outer electrons of Ti ( $3p^6, 4s^2, 3d^2$ ) and six of O ( $2s^2, 2p^4$ ) were explicitly treated. The number of  $k$  points ( $K_i$ ) in the Monkhorst–Pack<sup>77</sup>

sampling grid in both slab dimensions ( $i = x$  and  $i = y$ ) was chosen so that the product with the corresponding system dimension ( $S_i$ ) was 30 Å ( $K_i \approx 30 \text{ \AA}/S_i$ ) and one  $k$  point was used perpendicular to the slabs ( $K_z = 1$ ).

For the final minimization and density of states analysis, a higher number of  $k$  points ( $K_i \approx 80 \text{ \AA}/S_i$ ) was used, and the electron–ion interactions for Ti and O atoms were described by the projector-augmented wave (PAW) method developed by Blöchl<sup>78</sup> with the PBE<sup>79</sup> approximation for the exchange and correlation. In contrast to the ultra soft pseudopotential, the  $3s^2$  electrons of Ti are treated explicitly. For appropriate modeling of the electronic structure of atomic defects at the Ti/TiO<sub>2</sub> interface, the DFT+U approach was applied with  $U = 4 \text{ eV}$ .<sup>42</sup>

Full optimization of the lattice parameters and fractional coordinates was performed for bulk anatase, rutile, and metallic titanium. The calculated lattice parameters,  $a = 4.655 \text{ \AA}$  and  $c = 2.973 \text{ \AA}$  for rutile and  $a = 3.809 \text{ \AA}$  and  $c = 9.727 \text{ \AA}$  for anatase, are 0.4–2.5% higher than the respective experimental values ( $a = 4.587 \text{ \AA}$  and  $c = 2.959 \text{ \AA}$  for rutile and  $a = 3.782 \text{ \AA}$  and  $c = 9.502 \text{ \AA}$  for anatase<sup>80</sup>). Consequently the Ti–O bond lengths, 2.01 Å (apical) and 1.96 Å (basal) for both rutile and anatase, are slightly larger than the corresponding experimental ones (1.98 (apical) and 1.93 (basal)<sup>80</sup>). For titanium metal the calculated lattice parameters  $a = 2.949 \text{ \AA}$  and  $c = 4.690 \text{ \AA}$  were slightly larger than the experimental ones ( $a = 2.930 \text{ \AA}$  and  $c = 4.64405 \text{ \AA}$ <sup>81</sup>).

Surface and interface energies were calculated from differences of total energies, which were both calculated for minimized structures and by averaging the last 0.5 ps of free molecular dynamics.

The surface energies ( $\gamma_{\text{surf}}$ ) of Ti (0001), rutile (110), rutile (100), anatase (101), and anatase (001) were calculated from the total energies of the bulk system ( $E_{\text{bulk}}$ ) and of the respective half filled simulation cell ( $E_{\text{surf}}$ ) with the same heights and areas  $A$  as  $\gamma_{\text{surf}} = (E_{\text{surf}} - 2E_{\text{bulk}})/2A$ . Titanium is modeled by four layers of the hexagonal structure, and the surface is the closest packed plane (0001). As a model for the passivation layer, we constructed TiO<sub>2</sub> slabs of rutile in (100) and (110) orientations and anatase in (101) and (001) orientations. The slabs were oxygen terminated and had no dipole moment. Thicker slabs give a better representation but demand a higher computational effort. A compromise that well reproduces surface energy and the atomic charges is reached at four titanium layers for the anatase surfaces<sup>82</sup> and for rutile (100). For rutile (110) two layers resulted in a similar thickness.

To model the interface, supercell parameters had to be found that are commensurate with titanium and oxide lattices. The respective sizes of the TiO<sub>2</sub> and titanium slabs shown in Figure 1 match within a few percent in the  $x$  and  $y$  directions. Since agreement is never perfect, the final cell parameter was averaged between oxide and metal (see Figure 1).

The interface supercells are modeled as finite-thickness slab models with three-dimensional periodicity each consisting of a TiO<sub>2</sub> slab and a Ti slab of appropriate size. The noncontacting surfaces of metal and oxide are separated by vacuum with a thickness of at least 10 Å. The unit cell of metallic Ti is so small compared to the repetitive units on the TiO<sub>2</sub> surfaces, that translational fitting is negligible. For each of the four interfaces (Figure 1), three systems with identical box sizes and  $k$  points were set up, i.e., the combined system and the two isolated systems, containing metal or oxide only.

All twelve systems were subjected to Born–Oppenheimer molecular dynamics simulations with a 1 fs time step. The

lowest layer of the titanium metal slabs was fixed in  $z$  direction in all simulations with metal to preserve the calculated bulk parameters, whereas all other atoms are fully relaxed. To get comparable energy values all systems were treated with the same electronic smearing of 0.1 eV.<sup>83</sup> The systems were heated from 40 to 300 K within 0.2 ps and then subjected to free dynamic simulation for 2 ps at 300–500 K (temperature was rescaled to 300 K after 1 ps via Nosé-thermostat). For some of the systems, the temperature was increased to 1000 K and the simulation time doubled, to check that the system was equilibrated. The final structure was minimized and the density of states (DOS) was calculated. For the projected localized DOS (LDOS) Wigner Seitz radii of 1.2 Å were used, both for titanium and oxygen.

The work of separation was evaluated as  $W_{\text{sep}} = (E_{\text{Ti}} + E_{\text{TiO}_2} - E_{\text{Ti,TiO}_2})/A_c$ , where  $E_{\text{Ti}}$ ,  $E_{\text{TiO}_2}$ , and  $E_{\text{Ti,TiO}_2}$  are the total energies of the isolated relaxed metal and oxide systems and of the complete metal/oxide structures, respectively, and  $A_c$  is the area of contact.<sup>84</sup>

As the contact between the two phases replaces the surfaces to vacuum, the surface energies of metallic titanium ( $\gamma_{\text{Ti}}$ ) and the oxide ( $\gamma_{\text{TiO}_2}$ ) contribute to the interface energy which is given as  $\gamma_{\text{Ti,TiO}_2} = -W_{\text{sep}} + \gamma_{\text{surf,Ti}} + \gamma_{\text{surf,TiO}_2}$ .

Values for atomic charges were taken from the Bader charge analysis tool.<sup>85–87</sup> Charge density perpendicular to the slab was summed up from the CHGCAR file and normalized by  $A_c$ . Utilizing the dipole correction of VASP, the work function  $\Phi$  can be calculated as the difference between Fermi energy and vacuum level given in the OUTCAR file. The Fermi level of a semiconductor is located inside the band gap, but the position cannot be defined precisely from calculations without gap states. The local density of states (LDOS) was calculated in a VASP single-point calculation with fixed charge distribution. The number of considered bands was not sufficient to reproduce the virtual states well above the Fermi energy. These states were calculated with a reduced number of  $k$ -points and fitted to the DOS plots with higher number of  $k$ -points ( $K_i \approx 40 \text{ \AA}/S_i$ ), thus preserving the accuracy of the lower states.

Visualization of atomic structures was done with the program VMD (<http://www.ks.uiuc.edu/Research/vmd/>).<sup>88</sup>

### 3. RESULTS AND DISCUSSION

**3.1. Structures of Interfaces.** When the 2-fold coordinated oxygen atoms of the TiO<sub>2</sub> phase get in contact with Ti metal, they tent to occupy bridging or hollow positions on the metal and to form strong bonds. This weakens the bond with the oxide phase. Since the most favorable positions are on a hexagonal grid with only 1.7 Å distances between the lattice points, the O atoms displace almost perpendicularly to the metal surface and their final positions are determined mostly by the oxide structure. Due to the strong interaction between these oxygen atoms and the metal, some atoms are pulled out of the Ti surface by up to 0.4 Å and bind to two to three oxygen atoms. In all cases the structural perturbations are limited to the first layer of the metal and to the bottom layers of the oxide. Only in anatase (101) also higher layers are affected.

**3.1.1. Rutile (110).** In the  $y$  direction, the structure of oxide and metal are commensurate atom by atom. The 2-fold coordinated oxygen atoms are trapped in hollow and bridging positions depending on the relative shift in the  $x$  direction. In hollow positions they form three equal bonds of 2.2 Å to the

metal, pushing its surface atoms aside and increasing the distance between Ti rows in the  $\alpha$  direction by 0.6 Å. Those 3-fold coordinated surface oxygen atoms which are located above a hollow position in the  $\alpha$  direction displace toward the metal and form three identical bonds of 2.4 Å to the surrounding Ti atoms.

**3.1.2. Rutile (100).** Most of the rutile structure remains stable, but the interface oxygen layers are attracted by the metal Ti atoms some of which are pulled out of the surface layer. The 2-fold coordinated oxygen atoms maintain their bonds to Ti atoms in the oxide and bind to three atoms in the metal, thus interacting more strongly with the metal than with their original environment. Even some 3-fold coordinated oxygen atoms are attracted by the metal and pulled out of the rutile structure. Subsequently, oxygen atoms farther away from the interface relax toward these partial vacancies during dynamic simulation, but most of this structural perturbation is healed during final minimization. The oxygen migration leads to compression of the rutile structure close to the interface. Though the rutile Ti atoms are only slightly displaced, the atom layers of the oxide close to the metal have lost rutile structure.

**3.1.3. Anatase (101).** Surface oxygen atoms attach to the metal in bridging positions. The two bottom layers of anatase titanium atoms merge into one that mimics the structure of Ti metal. This leads to a slight change of the above structure, and the distance between the upper two Ti layers of anatase decreases from 0.9 Å to 0.6 Å. The distance between the merged bottom layer and the metal is less than 3 Å, which is in the range of atomic Ti–Ti distances, but still a partially filled oxygen layer is embedded between oxide and metal.

At the interface each anatase Ti atom is positioned directly above a metallic one, the rows matching perfectly in  $x$ -direction. In  $y$ -direction the metal Ti atoms are more closely packed and only three of four of them are “paired” with anatase Ti atoms.

**3.1.4. Anatase (001).** Some oxygen atoms penetrate the metal surface and form a bond to a second layer metal atom in addition to three bonds to atoms of the first metal layer. This is accompanied by displacement of one titanium atom out of the surface toward the oxide, while the other surrounding titanium atoms are pushed deeper into the metal. This strong structural relaxation nearly leads to mixing of metal and oxide titanium atoms as the lowest oxide titanium atom and the highest metal atom are approximately at the same height. 2-fold coordinated oxygen atoms at the surface to vacuum (both in the combined and separated system) show the tendency to temporarily detach from one of the two titanium atoms leaving an oxygen vacancy there. This should result in an energetically unfavorable surface structure. The final minimization restores 2-fold coordination, but the softening of the bond may give rise to a perturbation of the electronic structure.

**3.2. Work of Separation and Interface Energy.** Figure 3 shows the changes in total energy of separated and combined systems during the dynamic simulation. During the first steps the interface oxygen atoms moved quickly to the metal and nearly lost contact to the oxide, before the other oxide atoms followed. The oscillations especially in the upper energy curves after 0.2 ps reflect phonons of the pure metal. After 1.05 ps the temperature was rescaled to 300 K by Nosé-thermostat, which resulted in damping of the lattice oscillations especially in the separated systems. In the combined systems, potential interaction energy had been converted into thermal energy increasing the temperature significantly during the first

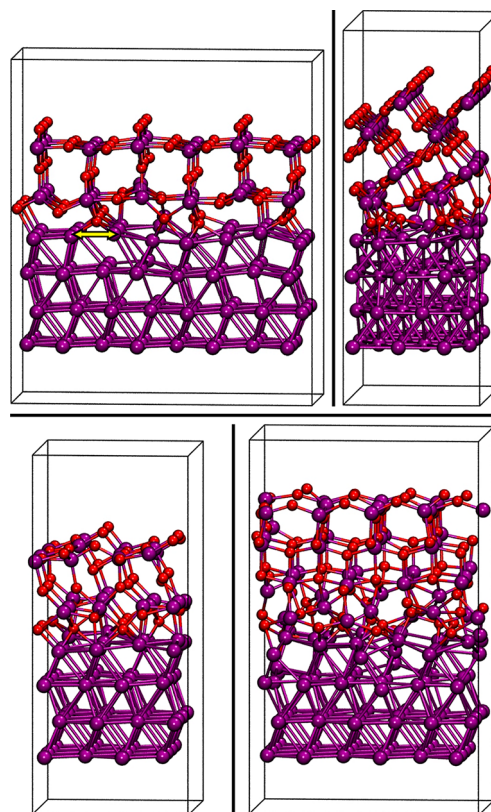


**Figure 2.** Final relaxed and minimized structures of  $\text{TiO}_2$  slabs on titanium metal (magenta, Ti; red, O): rutile (110) (top, left), rutile (100) (top, right), anatase (101) (bottom, left), and anatase (001) (bottom, right). The dimensions are the same as in Figure 1. The view along the  $y$  axis is shifted by 5° in  $x$  and  $z$  directions.

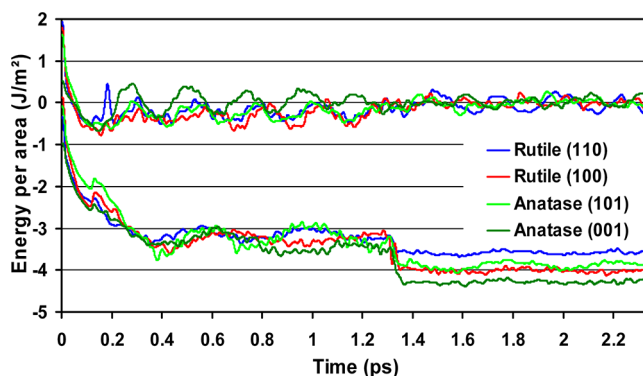


**Figure 3.** Sum of energies for oxide and metal (upper curve) and energy of oxide on metal (lower curve) for the four interfaces. For each interface, the work of separation is the difference between the respective lower and upper curves with and without interaction between oxide and metal. All energies have been normalized by the area of contact and aligned relative to the mean value of the relaxed isolated systems.

picosecond. Here temperature control induced a significant drop of the energy.

The work of separation ( $W_{\text{sep}}$ ) for each interface was averaged over the last 0.5 ps and calculated from optimization of the respective final structures (Table 1). There are reasons why dynamic calculations (Figure 3) are preferable to energy minimizations: (i) A continuous drift of the energy before equilibration can be distinguished from fluctuation around the

**Table 1. Calculated Works of Separation, Surface Energies, and Interface Energies in J/m<sup>2</sup><sup>a</sup>**

	$W_{\text{sep}}$	$\gamma_{\text{surf}}$	$\gamma_{\text{Ti,TiO}_2}$
rutile (110)	3.56 (3.42)	0.65 (0.67)	-0.92 (-0.69)
rutile (100)	4.04 (3.71)	0.93 (1.04)	-1.11 (-0.61)
anatase (101)	3.91 (3.67)	0.66 (0.76)	-1.26 (-0.85)
anatase (001)	4.31 (4.24)	1.52 (1.36)	-0.80 (-0.83)
titanium (0001)		1.99 (2.06)	

<sup>a</sup> $W_{\text{sep}}$  is the calculated work of separation to Ti (0001),  $\gamma_{\text{surf}}$  is the surface energy, and  $\gamma_{\text{Ti,TiO}_2}$  is the interface energy; values in brackets were obtained via optimization.

equilibrium. Figure 3 shows that the total energy converges within the simulated time scale. (ii) In a dynamic calculation, the respective energies are taken from averages over a number of similar configurations rather than from the single end point of an optimization, and a statistical error may be appreciated. In our case the values for  $W_{\text{sep}}$  were averaged over the last 0.5 ps corresponding to 500 configurations (Table 1), and the sample standard deviation of 0.09–0.16 J/m<sup>2</sup> is lower than the inherent bias of LDA simulations. (iii) Thermal atomic motions at a realistic temperature are introduced, whereas the minimization is in general considered to correspond to 0 K.

Here, works of separation from dynamics increase in the same order as from minimization (Table 1, first column) but are systematically higher by 0.1–0.3 J/m<sup>2</sup>. This is driven by

close contacts between oxide O and metal Ti atoms, which are more numerous when the oxide structure is softened by thermal motion. As optimization does not include thermal motion, the respective structures have higher order, and the contacts of O atoms in titanium oxide with Ti in the metal are not as favorable as in dynamics, where higher temperature enables farther displacement of the atoms from their lattice points.

Surface energies were calculated via optimization and dynamic simulation, as well. They are nearly equal in both approaches and well in the range of published data obtained via LDA calculations.<sup>89,90</sup> Furthermore the relation between the surfaces agrees with data obtained via PBE calculations.<sup>91,92</sup> The surface energy of solid titanium (2 J/m<sup>2</sup>) is higher than the experimental value for liquid titanium, 1.6 J/m<sup>2</sup>,<sup>93,94</sup> as might be expected. From these surface energies and the values for  $W_{\text{sep}}$  interface energies are obtained (Table 1).

For typical systems the interaction between different phases is energetically less favorable than in the pure bulk, and interface energies are positive. In the Ti/TiO<sub>2</sub> case the high values for  $W_{\text{sep}}$  result in significantly negative values of  $\gamma_{\text{Ti,TiO}_2}$  in all cases. Variations of interface energies between optimization and dynamics are solely caused by differences in  $W_{\text{sep}}$ . The surface energies  $\gamma_{\text{surf}}$  are very close for static and dynamic calculations, as the resulting structures are rather similar.

The work of separation for oxide in contact with metal is higher than for oxide–oxide separation ( $2\gamma_{\text{surf,oxide}}$ ) and almost

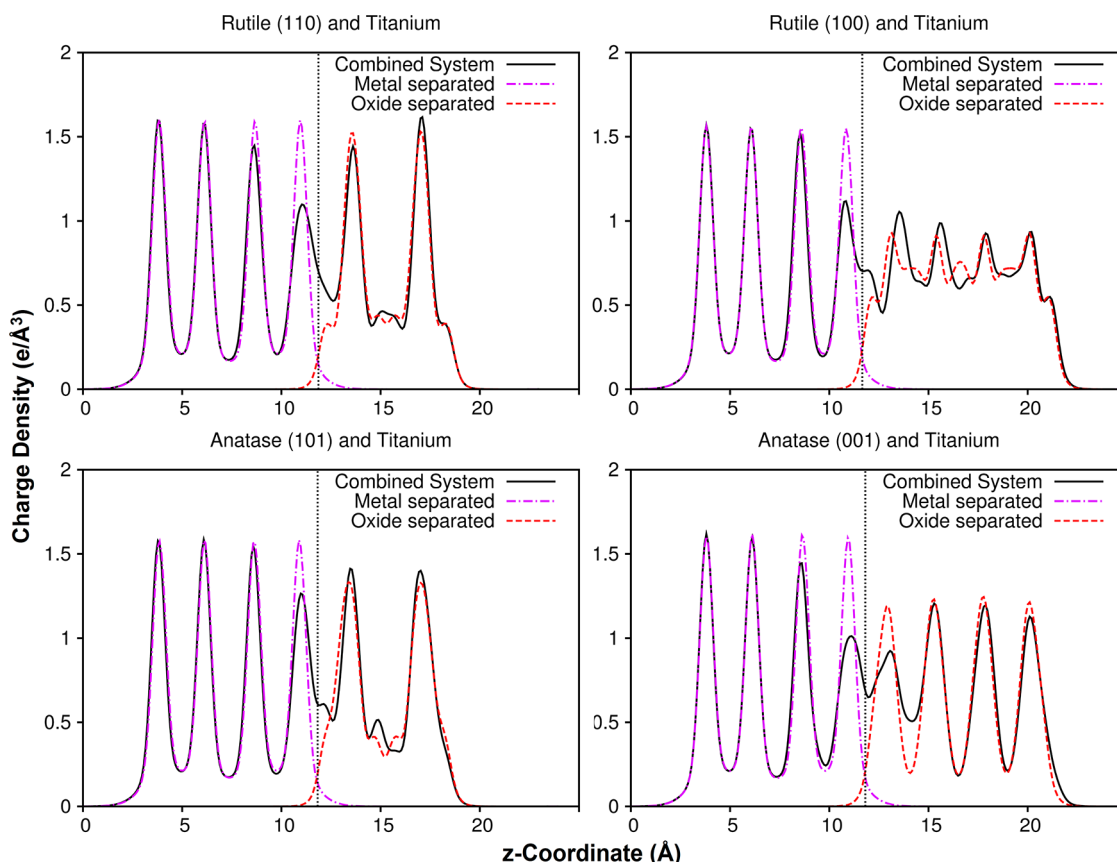


**Figure 4.** Electron density (e/Å<sup>3</sup>) perpendicular to the slabs. The curve for separated oxide (blue) has been aligned to the corresponding part of the combined curve (red). The separated metal curve (green) was not aligned as the bottom layer was constrained to one z-coordinate, both in the combined and separated systems. The dashed line indicates the fictitious borderline of volume assignment between metal and oxide for the combined system, defined by the intersection of the electron densities of the two noninteracting phases.

as high as for metal–metal ( $\sim 4 \text{ J/m}^2$ ). Consequently the contact between metal and interface region is very tight and applying mechanical force would rather lead to rupture within the  $\text{TiO}_2$  phase than within the interface region. This agrees with the rapid initial motion of the interface oxygen atoms.

**3.3. Charge Transfer (CT).** across metal/nonmetal interfaces has influence on the properties of the interface and the work function. The CT can be quantified by integration of the total charge distribution perpendicular to the oxide/metal interface, if its position is well-defined. We first positioned the electron densities of the separated systems to fit best to the respective parts of the combined systems. Then a border (cf. Figure 4) was defined thus that summing up the electron density of the two separated systems would result in zero charge transfer. The charge transfer at the simulated interface is calculated by integrating the difference between the curves of the combined and the separated systems on both sides of the dashed line (Table 2).

**Table 2. Total Charge Transfer, Calculated by Integrating the Charge Density over the Respective Volumes or by Summing up the Bader Charges<sup>a</sup>**

	$\int q_{\text{dens}}/A (\text{e/nm}^2)$	$\Sigma q_{\text{Bader}}/A (\text{e/nm}^2)$	$\Sigma q_{\text{Bader}}/N (\text{e})$
rutile (110)	3.54	7.91	0.069
rutile (100)	10.62	9.82	0.070
anatase (101)	2.42	7.92	0.071
anatase (001)	11.72	10.23	0.076

<sup>a</sup>  $\int q_{\text{dens}}/A$  is the integrated charge density per area,  $\Sigma q_{\text{Bader}}/A$  is the sum of Bader charges per area, and  $\Sigma q_{\text{Bader}}/N$  is the sum of Bader charges per total number of atoms (metal and oxide).

This method describes the polarization of an interface but does not correspond to chemical intuition, since not only change in population of orbitals results in charge transfer but also a full or partial crossing of the border by an atom due to structural relaxation of oxide and metal in contact with each other.

An alternative approach that is not based on a predefined border between the two phases is summing up the Bader charges of metal and oxide separately (Table 2). In all isolated systems some electron density is shifted from the surface toward the bulk (Figure 5, left). This effect occurs on top and bottom metal surfaces and seems to be independent of atomic relaxation, as the  $z$  coordinates of all bottom layer atoms are constrained to the same value. Consequently, all metal bulk layers have a total charge slightly above zero, and all surface layers slightly below, although fluctuations of the atomic charges occur within the layers. In the isolated oxide, oxygen charges are around  $-1.2$  in bulk and  $-1.0$  at the surface, and titanium charges are between  $+2.3$  and  $+2.4$  (Figure 5, left). In all four combined systems (Figure 5, right) the interface oxygen atoms draw electron density from the metal and reach charges around  $-1.4$ . The Ti atoms that are pulled out of the metal surface attain charges above  $+1.0$  (Figure 4, bottom). Most of the transferred charge remains close to the interface and is located by 66–83% in the first interface layer. Bader charge transfer values (Table 2) for the very stable surfaces rutile (110) and anatase (101) are significantly larger than from the integration method ( $8 \text{ vs } 3 \text{ e/nm}^2$ ), whereas for rutile (100) and anatase (001) similar values around  $10 \text{ e/nm}^2$  are obtained from both methods. In our limited number of samples, high charge transfer seems to correlate with high surface energy

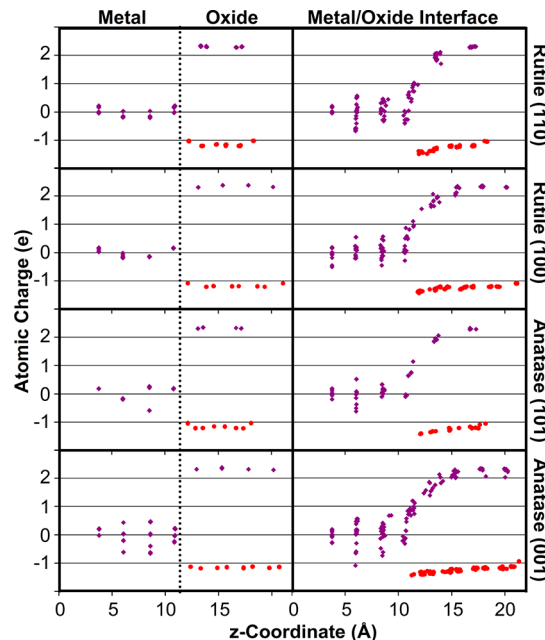


**Figure 5.** Atomic charge distribution along the  $z$  coordinate. Each point represents one atom at the given height (Ti, magenta diamonds; O, red circles). Metal and oxide on the left side are noninteracting. The position of the oxide crystal was aligned to match its position in the metal/oxide interface. On the right side the charges are displayed, which result from interaction between metal and oxide.

(Table 1) and vice versa. Still the total charge transfer (CT) as calculated from Bader charges is around 0.07 electrons per atom, indicating that the charge transfer for all four interfaces might scale with slab thickness. It is relevant for the following discussion of the change in work function that the CT is similar in value for all four interfaces.

**3.4. Density of States.** The density of electronic states (DOS) of pure bulk titanium (see the Supporting Information) showed good agreement with published data.<sup>81</sup> Scaling the lattice parameters of the metal to fit the oxides (Figure 1) had no significant effect on the DOS (Figure 6, blue).

With respect to the respective bulk, the states of surface atoms both in metal and oxide show a slight shift of weight toward higher energies, resulting in lower electron occupation at the surface. This effect leads to a small displacement of charge (Figure 5, left) as discussed above. These observations agree with the calculations of  $\text{TiO}_2$ <sup>82</sup> where the outer layers had higher states than the inner ones, both for relaxed (1 and 2) and constrained surfaces (3 and 4). In the anatase (101) slab all titanium layers have almost the same distance to the surface and show very similar DOS. Surface layers of the metal have about twice as much density of states around the Fermi energy and up to 1 eV above it, compared to bulk layers.

The calculated bulk band gaps are 2.0 eV (Figure 6) for rutile and 2.3 eV for anatase, which is in good agreement with other theoretical works.<sup>29–31</sup> All slabs have the same band gap as the corresponding bulk system, with the exception of anatase (001). Oxygen atoms in this less stable surface produce states above the valence band reducing the gap to 1.3 eV. This agrees with the partial detachment of 2-fold coordinated oxygen atoms at the anatase (001) surface discussed above.

When the contact of the metal and oxide phases is established, the characteristic features of the total DOS for oxides and metals are maintained, but the weights are shifted

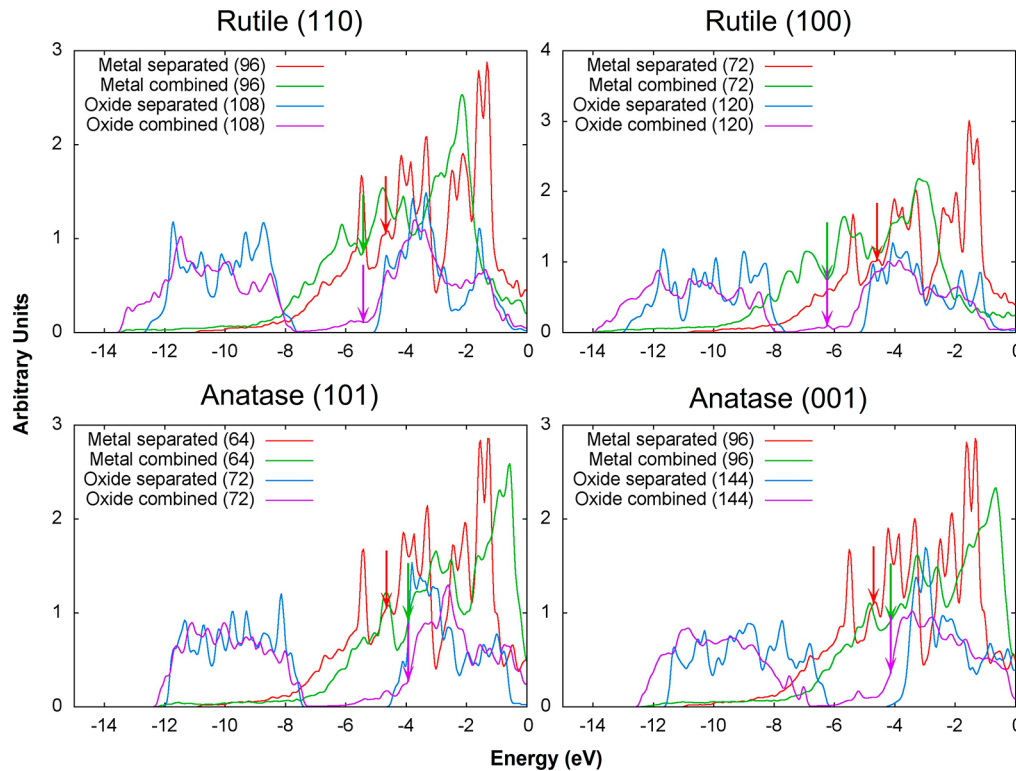


**Figure 6.** Projected density of states (LDOS) of the metal and oxide phases both combined and separated (numbers of atoms in brackets). The energy scale was chosen relative to the vacuum value of the work function, where  $E = 0$  is the energy of a free electron and the Fermi levels are indicated by arrows. For separated oxides the Fermi level cannot be calculated.

**Table 3. Calculated Change of Work Functions for Ti Metal and  $\text{TiO}_2/\text{Ti}$  Interfaces and Position of the Top of the Valence Band and Bottom of the Conduction Band in the Isolated Oxide Phases (in eV)<sup>a</sup>**

	$\Phi(\text{Ti})$	$\Phi(\text{TiO}_2/\text{Ti})$	$\Delta\Phi$	top VB $\text{TiO}_2$	bottom CB $\text{TiO}_2$
rutile (110)	4.71	5.44	0.73	-7.35	-5.35
rutile (100)	4.63	6.28	1.65	-7.32	-5.44
anatase (101)	4.66	3.95	-0.71	-7.13	-4.89
anatase (001)	4.74	4.16	-0.58	-5.87	-4.58

<sup>a</sup>The work function for the combined systems is calculated at the oxide side, as the titanium is in general covered by an oxide layer, and electrons can leave the surface only via the oxide.

toward lower energies inside each band. The observed modifications of the DOS are related to significant structural relaxation at the interface (Figure 2 and 5). Only the projected DOS of atoms close to the interface are affected, but the contribution to the total DOS is significant. In the oxides, additional states are formed with energies of up to 2 eV below the original bottom of the valence band, which mainly belong to oxygen atoms at the interface. Both effects indicate a strong metal–oxide interaction and correlate with the high work of separation.

Metal induced gap states (MIGS) appear in the oxide (Figure 6). Some are spread evenly over the range of the gap. They are assigned to oxygen atoms forming bonds to the metal and may be comparable to those found at  $\text{Pt}/\text{TiO}_2$  interfaces.<sup>30</sup> Most MIGS, however, are located in the upper part of the gap less than 1 eV below the conduction-band. These states belong to titanium atoms in the oxide close to the interface and appear in the range of experimentally observed defect states created by oxygen vacancies.<sup>32,33</sup> Such states have appreciable weight in the interface layer only and decay strongly into the subinterface layer.

In the metal additional states are formed at the interface, and are found 6–8 eV below the Fermi level where the isolated systems have no states at all. This effect is limited to the atom layer closest to the surface and has little effect on the total DOS. The sharp peaks of the separated slab with two similar surfaces are smoothed when one surface is replaced by the interface with the oxide and the slab symmetry is significantly reduced.

**3.5. Work Functions.** Changes in work function induced by an oxide thin film on a metal have very important consequences for a number of phenomena.<sup>95</sup> This is particularly relevant for ultrathin films, like the ones considered in this work. In fact, in this case a communication between the metal support and the oxide surface or species adsorbed on the oxide surface can take place via direct electron tunneling through the thin insulating layer.<sup>95</sup> For this reason we have discussed in particular changes in the metal work function due to the growth of the oxide thin layer. Of course, if the oxide phase becomes much thicker than the films considered here the work function of the  $\text{TiO}_2$  surface becomes the relevant feature.

Small differences in the work function (Table 3) of pure titanium metal are ascribed to the slightly different lattice

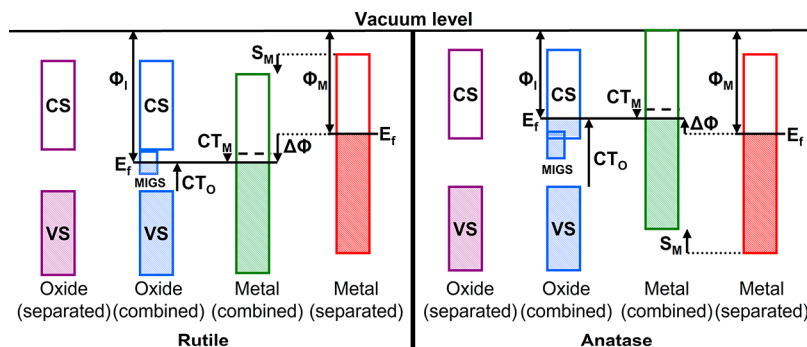


**Figure 7.** Schematic diagram of the different work function trends for rutile and anatase. CB, conduction band; VB, valence band;  $CT_O$  and  $CT_M$ , change in occupation of oxide and metal due to charge transfer,  $S_M$ , shift of metal states due to polarization and charge compression ( $S_M = CT_M + CC_M$ );  $\Phi_I$  and  $\Phi_M$ , work functions of interface system and metal;  $E_f$ , Fermi level.

parameters used in the calculations. Sample calculations showed that the work function is almost inversely proportional to the change in metal density within a few percent (Figure 1, scaling factors). Our results for Ti (0001) are close to experimental (4.6 eV<sup>45,46</sup>) and theoretical (4.45 eV<sup>52</sup>) values reported in the literature. An important aspect of metal/oxide interfaces is the change in work function. Upon deposition of the  $TiO_2$  slab on Ti,  $\Phi$  changes in different ways, depending on the structure of the oxide phase. In particular  $\Phi$  increases for rutile and decreases for anatase (Table 3). This change of work function,  $\Delta\Phi$ , does not correlate directly with the amount of charge transferred (CT) shown in Table 2.

The positions of top of the VB and bottom of CB in the titania films are not significantly shifted relative to vacuum level for the more stable surfaces rutile (110) and anatase (101), while they are downshifted by less than 0.5 eV for the other two structures (Figure 6 and 7). Due to the presence of MIGS, the Fermi level is now defined in the oxide band gap.

Before the contact between Ti and  $TiO_2$  is established and electronic relaxation takes place, all initial oxide work functions are higher than that of the Ti metal. Thus, for energetic reasons, charge transfer occurs from metal to oxide. This CT changes the electronic occupation in the two phases. In the metal upper states are depopulated and the Fermi level is downshifted relative to its electronic DOS ( $CT_M$ ). In the oxide additional states are filled (especially the MIGS) and the Fermi level rises relative to the oxide DOS ( $CT_O$ ). (The shift of the DOS relative to the vacuum level that further affects the final Fermi energy is discussed below.) Since the density of states around the Fermi level in the metal is much higher than in the oxide, a given CT leads to a small decrease of the Fermi level in the metal and a larger increase in the oxide (Figure 7,  $CT_O > CT_M$ ).

The CT has a similar amount for all interfaces (Table 2), but rutile and anatase respond differently to it. In rutile all MIGS lie in the band gap<sup>29</sup> and take up all transferred electrons resulting in a final Fermi level in the former band gap. In anatase half of the metal induced states are located in the conduction band,<sup>29</sup> and there is not sufficient density of states in the band gap to take up all transferred electrons. As a consequence states in the conduction band are filled, which leads to a higher final Fermi level. (Figure 6 and 7). As CT fills up the MIGS and in anatase some of these states are located around the bottom of the CB, the Fermi energy is close to this level (within 1 eV) (Table 3). This is consistent with the approximate correlation of the work functions and the position of the bottom of the CBs.

During contact with  $TiO_2$ , the Fermi levels of the metal have to equilibrate with that of the oxide. The reorganization of charge stops when the work function for oxide and metal reach the same level and the Fermi energies are equal (Figure 7).

The main contributions to  $\Delta\Phi$  are shifts of the electronic states relative to vacuum level. The charge transfer (CT) from metal to oxide generally enhances  $\Phi$ , but is balanced by the second relevant process, charge compression (CC) of the metal near the interface (Figure 7,  $CC_M$ ). From our data on electron density (Figure 4) no significant differences in charge compression between the four interfaces could be discerned.

The CT reduces the occupation in the metal as described above which causes a reduction of the work function ( $CT_M$ ), but the transferred charge also shifts the states relative to vacuum level. Since the electrons are not distributed equally in the oxide (Figure 4), a polarization ( $CT_p$ ) is induced that reduces the work function. This second effect only occurs when the semiconducting film on the metal has a certain thickness. In our systems the amount of transferred charge was similar (Table 2), but its effect on the Fermi level, and thus on the work function, differed significantly. According to Figure 7, rutile induces a downshift to match its Fermi level inside the gap, whereas anatase affords an upshift for equilibrating with its Fermi level within the CB.

#### 4. CONCLUSIONS

In this work we have considered the properties of sharp interfaces formed between Ti metal and a  $TiO_2$  layer consisting of rutile or anatase with two different surface terminations for each oxide phase. In all cases the work of separation is higher than the sum of surface energies, indicating the formation of an energetically very favorable interface region that glues the two phases together. The interface energy is negative, which means that for Ti and  $TiO_2$  bulk phases mixing is energetically favorable.

The influence of the metal on the atomic and electronic structure of the oxide is limited to a few atomic layers. In atomistic simulations aiming at a realistic surface of  $TiO_2$ , the influence of the underlying metal can be neglected as long as the shifts of work function and small charge transfers from the metal to the oxide do not play an important role.

MIGS in the band gap of  $TiO_2$  have appreciable weight in the Ti/ $TiO_2$  interface layer only and decay strongly into the subinterface layer. Depending on its modification a passivation layer may give rise to up- (rutile) or downshift (anatase) of the work function of the underlying titanium metal. Consequently

the work function of titanium may not be very well-defined in practice.

We confirm the occurrence of delocalized gap states in anatase and show that they are not only induced by oxygen vacancies, but also by the presence of an excess of Ti atoms at the metal-oxide interface. These states are possibly relevant for the photosensitivity of passivated titanium.<sup>29,73</sup>

## ■ ASSOCIATED CONTENT

### § Supporting Information

Includes seven plots of total and projected density of states (DOS and LDOS) that illustrate details of interest for the discussed interfaces: bulk titanium, separated titanium slab, titanium slab with contact to TiO<sub>2</sub>, rutile bulk and slabs, anatase bulk and slabs, and oxygen atoms in anatase (001). This material is available free of charge via the Internet at <http://pubs.acs.org>.

## ■ AUTHOR INFORMATION

### Corresponding Author

\*E-mail: langel@uni-greifswald.de.

### Notes

The authors declare no competing financial interest.

## ■ ACKNOWLEDGMENTS

We thank COST for sponsoring the conferences that brought us together in the course of the D41 action. The Greifswald group acknowledges gratefully the support of the Deutsche Forschungsgemeinschaft (DFG Project La700/8-2). B.O. would like to thank COST for financing his 5 weeks stay at the Università degli Studi di Milano Bicocca and the whole group of G. Pacchioni for their great hospitality. Further thanks go to Norman Geist for improving the performance of VASP on the computational resources in Greifswald and to Prof. Lucio Colombi Ciacchi (Bremen) for fruitful discussions. The work of G. P. and S. P. is supported from the Italian MIUR through the FIRB Project RBAP11SAYN “Oxides at the nanoscale: multifunctionality and applications”.

## ■ REFERENCES

- (1) Lausmaa, J.; Kasemo, B.; Mattsson, H. *Appl. Surf. Sci.* **1990**, *44*, 133–146.
- (2) da Fonseca, C.; Boudin, S.; Belo, M. D. *J. Electroanal. Chem.* **1994**, *379*, 173–180.
- (3) Sul, Y. T.; Johansson, C. B.; Petronis, S.; Krozer, A.; Jeong, Y.; Wennerberg, A.; Albrektsson, T. *Biomaterials* **2002**, *23*, 491–501.
- (4) Wu, Q.-H.; Fortunelli, A.; Granozzi, G. *Int. Rev. Phys. Chem.* **2009**, *28*, 517–576.
- (5) Bignolas, J. B.; Bujor, M.; Bardolle, J. *Surf. Sci.* **1981**, *108*, L453–L459.
- (6) Bertel, E.; Stockbauer, R.; Madey, T. E. *Surf. Sci.* **1984**, *141*, 355–387.
- (7) Lee, P. A.; Stork, K. F.; Maschhoff, B. L.; Nebesny, K. W.; Armstrong, N. R. *Surf. Interface Anal.* **1991**, *17*, 48–56.
- (8) Oviedo, C. *J. Phys.: Condens. Matter* **1993**, *5*, A153–A154.
- (9) Vaquila, I.; Passeggi, M. C. G.; Ferron, J. *Appl. Surf. Sci.* **1996**, *93*, 247–253.
- (10) Azoulay, A.; Shamir, N.; Fromm, E.; Mintz, M. H. *Surf. Sci.* **1997**, *370*, 1–16.
- (11) Lu, G.; Bernasek, S. L.; Schwartz, J. *Surf. Sci.* **2000**, *458*, 80–90.
- (12) Takakuwa, Y.; Ishidzuka, S.; Yoshigoe, A.; Teraoka, Y.; Mizuno, Y.; Tonda, H.; Homma, T. *Nuclear Instrum. Methods Phys. Res. Sect. B* **2003**, *200*, 376–381.
- (13) Takakuwa, Y.; Ishidzuka, S.; Yoshigoe, A.; Teraoka, Y.; Yamauchi, Y.; Mizuno, Y.; Tonda, H.; Homma, T. *Appl. Surf. Sci.* **2003**, *216*, 395–401.
- (14) Vergara, L. I.; Passeggi, M. C. G.; Ferron, J. *Appl. Surf. Sci.* **2002**, *187*, 199–206.
- (15) Vaquila, I.; Passeggi, M. C. G.; Ferron, J. *Surf. Sci.* **1993**, *292*, L795–L800.
- (16) Mayer, J. T.; Diebold, U.; Madey, T. E.; Garfunkel, E. *J. Electron Spectrosc. Relat. Phenom.* **1995**, *73*, 1–11.
- (17) Schneider, J.; Colombi Ciacchi, L. *Surf. Sci.* **2010**, *604*, 1105–1115.
- (18) Wang, J. H.; Lin, M. C. *ChemPhysChem* **2004**, *5*, 1615–1618.
- (19) Li, W.; Ni, C.; Lin, H.; Huang, C. P.; Shah, S. I. *J. Appl. Phys.* **2004**, *96*, 6663–6668.
- (20) Huang, W.-F.; Raghunath, P.; Lin, M. C. *J. Comput. Chem.* **2010**, *32*, 1065–1081.
- (21) Kim, K. D.; Kim, S. H.; Kim, H. T. *Colloids Surf. A* **2005**, *254*, 99–105.
- (22) Li, G. L.; Wang, G. H. *Nanostruct. Mater.* **1999**, *11*, 663–668.
- (23) Hwu, Y.; Yao, Y. D.; Cheng, N. F.; Tung, C. Y.; Lin, H. M. *Nanostruct. Mater.* **1997**, *9*, 355–358.
- (24) Zhang, H. Z.; Banfield, J. F. *J. Mater. Chem.* **1998**, *8*, 2073–2076.
- (25) Zhang, H. Z.; Banfield, J. F. *J. Phys. Chem. B* **2000**, *104*, 3481–3487.
- (26) Ranade, M. R.; Navrotsky, A.; Zhang, H. Z.; Banfield, J. F.; Elder, S. H.; Zaban, A.; Borse, P. H.; Kulkarni, S. K.; Doran, G. S.; Whitfield, H. J. *Proc. Natl. Acad. Sci. U.S.A.* **2002**, *99*, 6476–6481.
- (27) Enyashin, A. N.; Seifert, G. *Phys. Status Solidi B* **2005**, *242*, 1361–1370.
- (28) Linsebigler, A. L.; Lu, G. Q.; Yates, J. T. *Chem. Rev.* **1995**, *95*, 735–758.
- (29) Mattioli, G.; Filippone, F.; Alippi, P.; AmoreBonapasta, A. *Phys. Rev. B* **2008**, *78*, 241201.
- (30) Tamura, T.; Ishibashi, S.; Terakura, K.; Weng, H. *Phys. Rev. B* **2009**, *80*, 195302.
- (31) Vogtenhuber, D.; Podloucky, R.; Neckel, A.; Steinemann, S. G.; Freeman, A. *J. Phys. Rev. B* **1994**, *49*, 2099–2103.
- (32) Henderson, M. A.; Epling, W. S.; Peden, C. H. F.; Perkins, C. L. *J. Phys. Chem. B* **2003**, *107*, 534–545.
- (33) Kurtz, R. L.; Stockbauer, R.; Madey, T. E.; Roman, E.; Desegovia, J. L. *Surf. Sci.* **1989**, *218*, 178–200.
- (34) Serwica, E.; Schlierkamp, M. W.; Schindler, R. N. Z. *Naturforsch. Sect. A* **1981**, *36*, 226–232.
- (35) Berger, T.; Sterrer, M.; Diwald, O.; Knozinger, E.; Panayotov, D.; Thompson, T. L.; Yates, J. T. *J. Phys. Chem. B* **2005**, *109*, 6061–6068.
- (36) Hurum, D. C.; Agrios, A. G.; Gray, K. A.; Rajh, T.; Thurnauer, M. C. *J. Phys. Chem. B* **2003**, *107*, 4545–4549.
- (37) Cho, E.; Han, S.; Ahn, H.-S.; Lee, K.-R.; Kim, S. K.; Hwang, C. S. *Phys. Rev. B* **2006**, *73*, 193202.
- (38) Na-Phattalung, S.; Smith, M. F.; Kim, K.; Du, M. H.; Wei, S. H.; Zhang, S. B.; Limpijumnong, S. *Phys. Rev. B* **2006**, *73*, 125205.
- (39) Ganduglia-Pirovano, M. V.; Hofmann, A.; Sauer, J. *Surf. Sci. Rep.* **2007**, *62*, 219–270.
- (40) Pacchioni, G. *J. Chem. Phys.* **2008**, *128*, 182505.
- (41) Di Valentini, C.; Pacchioni, G.; Selloni, A. *Phys. Rev. Lett.* **2006**, *97*, 166803.
- (42) Finazzi, E.; Di Valentini, C.; Pacchioni, G.; Selloni, A. *J. Chem. Phys.* **2008**, *129*, 154113.
- (43) Morgan, B. J.; Watson, G. W. *Surf. Sci.* **2007**, *601*, 5034–5041.
- (44) Yang, Z. X.; Wu, R. Q.; Goodman, D. W. *Phys. Rev. B* **2000**, *61*, 14066–14071.
- (45) Feibelman, P. J.; Himpsel, F. J. *Phys. Rev. B* **1980**, *21*, 1394–1399.
- (46) Jonker, B. T.; Morar, J. F.; Park, R. L. *Phys. Rev. B* **1981**, *24*, 2951–2957.
- (47) Liu, S.-Y.; Wang, F.-H.; Zhou, Y.-S.; Shang, J.-X. *J. Phys.: Condens. Matter* **2007**, *19*, 226004.

- (48) Brearley, W.; Surplice, N. A. *Surf. Sci.* **1977**, *64*, 372–374.
- (49) Hanson, D. M.; Stockbauer, R.; Maday, T. E. *Phys. Rev. B* **1981**, *24*, 5513–5521.
- (50) Fukuda, Y.; Elam, W. T.; Park, R. L. *Appl. Surf. Sci.* **1978**, *1*, 278–287.
- (51) Brugniau, D.; Argile, C.; Bartheslabrousse, M. G.; Rhead, G. E. *Surf. Sci.* **1984**, *141*, 639–653.
- (52) Imanishi, A.; Tsuji, E.; Nakato, Y. *J. Phys. Chem. C* **2007**, *111*, 2128–2132.
- (53) Della Negra, M.; Nicolaisen, N. M.; Li, Z. S.; Moller, P. J. *Surf. Sci.* **2003**, *540*, 117–128.
- (54) Karuppasamy, A.; Subrahmanyam, A. *J. Appl. Phys.* **2007**, *101*, 064318.
- (55) Lenzmann, F.; Krueger, J.; Burnside, S.; Brooks, K.; Gratzel, M.; Gal, D.; Ruhle, S.; Cahen, D. *J. Phys. Chem. B* **2001**, *105*, 6347–6352.
- (56) Orlov, A.; Tikhov, M. S.; Lambert, R. M. *C. R. Chim.* **2006**, *9*, 794–799.
- (57) Emori, M.; Sugita, M.; Ozawa, K.; Sakama, H. *Phys. Rev. B* **2012**, *85*, 035129.
- (58) Prada, S.; Martinez, U.; Pacchioni, G. *Phys. Rev. B* **2008**, *78*, 235423.
- (59) Heine, V. *Phys. Rev.* **1965**, *138*, 1689–1696.
- (60) Louie, S. G.; Cohen, M. L. *Phys. Rev. B* **1976**, *13*, 2461–2469.
- (61) Bordier, G.; Noguera, C. *Phys. Rev. B* **1991**, *44*, 6361–6371.
- (62) Glaus, S.; Calzaferri, G.; Hoffmann, R. *Chem.—Eur. J.* **2002**, *8*, 1785–1794.
- (63) Yeo, Y. C.; King, T. J.; Hu, C. M. *J. Appl. Phys.* **2002**, *92*, 7266–7271.
- (64) Giordano, L.; Cinquini, F.; Pacchioni, G. *Phys. Rev. B* **2006**, *73*, 045414.
- (65) Leung, T. C.; Kao, C. L.; Su, W. S.; Feng, Y. J.; Chan, C. T. *Phys. Rev. B* **2003**, *68*, 195408.
- (66) Friedrichs, W.; Ohler, B.; Langel, W.; Monti, S.; Koeppen, S. *Adv. Eng. Mater.* **2011**, *13*, B334–B342.
- (67) Koeppen, S.; Ohler, B.; Langel, W. *Z. Phys. Chem.-Int. J. Res. Phys. Chem. Chem. Phys.* **2007**, *221*, 3–20.
- (68) Koeppen, S.; Langel, W. *Langmuir* **2010**, *26*, 15248–15256.
- (69) Koeppen, S.; Bronkalla, O.; Langel, W. *J. Phys. Chem. C* **2008**, *112*, 13600–13606.
- (70) Koppen, S.; Langel, W. *Phys. Chem. Chem. Phys.* **2008**, *10*, 1907–1915.
- (71) Koppen, S.; Langel, W. *Surf. Sci.* **2006**, *600*, 2040–2050.
- (72) Ohler, B.; Langel, W. *J. Phys. Chem. C* **2009**, *113*, 10189–10197.
- (73) Kresse, G.; Hafner, J. *Phys. Rev. B* **1993**, *47*, 558–561.
- (74) Kresse, G.; Furthmuller, J. *Phys. Rev. B* **1996**, *54*, 11169–11186.
- (75) Perdew, J. P.; Zunger, A. *Phys. Rev. B* **1981**, *23*, 5048–5079.
- (76) Monkhorst, H. J.; Pack, J. D. *Phys. Rev. B* **1976**, *13*, 5188–5192.
- (77) Blochl, P. E. *Phys. Rev. B* **1994**, *50*, 17953–17979.
- (78) Perdew, J. P.; Burke, K.; Ernzerhof, M. *Phys. Rev. Lett.* **1996**, *77*, 3865–3868.
- (79) Burdett, J. K.; Hughbanks, T.; Miller, G. J.; Richardson, J. W.; Smith, J. V. *J. Am. Chem. Soc.* **1987**, *109*, 3639–3646.
- (80) Raji, A. T.; Mazzarello, R.; Scandolo, S.; Nsengiyumva, S.; Haerting, M.; Britton, D. T. *Solid State Commun.* **2011**, *151*, 1889–1893.
- (81) Calatayud, M.; Minot, C. *Surf. Sci.* **2004**, *552*, 169–179.
- (82) Methfessel, M.; Paxton, A. T. *Phys. Rev. B* **1989**, *40*, 3616–3621.
- (83) Munoz, M. C.; Gallego, S.; Beltran, J. I.; Cerda, J. *Surf. Sci. Rep.* **2006**, *61*, 303–344.
- (84) Tang, W.; Sanville, E.; Henkelman, G. *J. Phys.: Condens. Matter* **2009**, *21*, 084204.
- (85) Sanville, E.; Kenny, S. D.; Smith, R.; Henkelman, G. *J. Comput. Chem.* **2007**, *28*, 899–908.
- (86) Henkelman, G.; Arnaldsson, A.; Jonsson, H. *Comput. Mater. Sci.* **2006**, *36*, 354–360.
- (87) Humphrey, W.; Dalke, A.; Schulten, K. *J. Mol. Graph. Modell.* **1996**, *14*, 33–38.
- (88) Lazzeri, M.; Vittadini, A.; Selloni, A. *Phys. Rev. B* **2001**, *63*, 155409.
- (89) Ramamoorthy, M.; Vanderbilt, D.; Kingsmith, R. D. *Phys. Rev. B* **1994**, *49*, 16721–16727.
- (90) Lazzeri, M.; Vittadini, A.; Selloni, A. *Phys. Rev. B* **2002**, *65*, 119901.
- (91) Diebold, U.; Ruzycki, N.; Herman, G. S.; Selloni, A. *Catal. Today* **2003**, *85*, 93–100.
- (92) Tille, J.; Kelly, J. C. *Br. J. Appl. Phys.* **1963**, *14*, 717–719.
- (93) Flint, O. *J. Nucl. Mater.* **1965**, *16*, 233–248.
- (94) Pacchioni, G. *Chem.—Eur. J.* **2012**, *18*, 10144–10158.
- (95) Giordano, L.; Pacchioni, G. *Acc. Chem. Res.* **2011**, *44*, 1244–1252.